Plant Physiology and Biochemistry 210 (2024) 108592

Contents lists available at ScienceDirect

Plant Physiology and Biochemistry

journal homepage: www.elsevier.com/locate/plaphy

Azelaic acid can efficiently compete for the auxin binding site TIR1, altering auxin polar transport, gravitropic response, and root growth and architecture in *Arabidopsis thaliana* roots

Sara Álvarez-Rodríguez [a,b], Fabrizio Araniti [c,*], Marta Teijeira [d,e], Manuel J. Reigosa [a,b], Adela M. Sánchez-Moreiras [a,b]

[a] Universidade de Vigo. Departamento de Bioloxía Vexetal e Ciencias do Solo, Facultade de Bioloxía, Campus Lagoas-Marcosende s/n, 36310, Vigo, Spain
[b] Instituto de Agroecoloxía e Alimentación (IAA). Universidade de Vigo - Campus Auga, 32004, Ourense, Spain
[c] Dipartimento di Scienze Agrarie e Ambientali - Produzione, Territorio, Agroenergia, Università Statale di Milano, Via Celoria n°2, 20133, Milano, Italy
[d] Departamento de Química Orgánica, Facultade de Química, Universidade de Vigo, 36310, Vigo, Spain
[e] Instituto de Investigación Sanitaria Galicia Sur, Hospital Álvaro Cunqueiro, 36213, Vigo, Spain

ARTICLE INFO

Keywords:
Azelaic acid
Auxin
Auxin polar transport
Gravitropism
TIR1

ABSTRACT

The present study investigates the phytotoxic potential of azelaic acid (AZA) on *Arabidopsis thaliana* roots. Effects on root morphology, anatomy, auxin content and transport, gravitropic response and molecular docking were analysed. AZA inhibited root growth, stimulated lateral and adventitious roots, and altered the root apical meristem by reducing meristem cell number, length and width. The treatment also slowed down the roots' gravitropic response, likely due to a reduction in statoliths, starch-rich organelles involved in gravity perception. In addition, auxin content, transport and distribution, together with PIN proteins' expression and localisation were altered after AZA treatment, inducing a reduction in auxin transport and its distribution into the meristematic zone. Computational simulations showed that AZA has a high affinity for the auxin receptor TIR1, competing with auxin for the binding site. The AZA binding with TIR1 could interfere with the normal functioning of the TIR1/AFB complex, disrupting the ubiquitin E3 ligase complex and leading to alterations in the response of the plant, which could perceive AZA as an exogenous auxin. Our results suggest that AZA mode of action could involve the modulation of auxin-related processes in *Arabidopsis* roots. Understanding such mechanisms could lead to find environmentally friendly alternatives to synthetic herbicides.

1. Introduction

For many years, synthetic herbicides have been considered the best alternative for weed management. However, their massive use has led to multiple environmental problems and the increase of many resistant weed species. For this reason, there has been growing interest in exploring new specialized metabolites, produced by allelopathic species among other organisms, with possible innovative modes of action and able to reduce weed resistance development (Qu et al., 2021).

These specialized metabolites produced by allelopathic species are also known as allelochemicals. Most of these compounds belong to three main chemical classes of plant specialized metabolites (terpenoids, phenolic acids and nitrogen compounds). However, they are characterised by showing different modes of action, with the potential of multi-target action, by affecting more than one molecular site in the plant metabolism (Grossmann et al., 2001). Recent studies highlighted the ability of these molecules to alter root meristem and its architecture, suggesting their possible interaction with different plant hormones, such as auxin, known for being involved in the maintenance of root structure and the processes of root growth and development (Gomes and Scortecci, 2021). Indeed, herbicides that mimic the natural auxin indole-3-acetic acid (IAA), considered as auxinic herbicides, have played an important role in weed control for many years and continue to be one of the most widely used today (Prusinska et al., 2023). The family of auxinic herbicides is formed by four main chemical groups: phenoxyacetic acids (e.g., 2,4-dichlorophenoxyacetic acid), benzoic acids (e.g., dicamba), pyridine carboxylic acids (e.g., picloram or clopyralid), and quinolinecarboxylic acids (e.g., quinclorac or quinmerac) (Song, 2014).

* Corresponding author.
E-mail address: fabrizio.araniti@unimi.it (F. Araniti).

https://doi.org/10.1016/j.plaphy.2024.108592
Received 27 January 2024; Accepted 31 March 2024
Available online 1 April 2024

The use of these auxinic herbicides has been significant in the history of weed management, and their widespread use has led to increase of resistant weed populations. Auxinic herbicides such as 2,4-D and dicamba have been reported to be resistant to some weed species. They are two of the most widely used herbicides, whose mechanism of action is based on binding to the auxin receptor TIR1 (Transport Inhibitor Response 1), resulting in overstimulation of the auxin response pathway (Song, 2014; Schulz and Segobye, 2016). The auxin receptor TIR (Transport Inhibitor Response 1) is an F-box protein that is part of the SCF (Skp1-Cullin-F-box) E3 ubiquitin ligase complex. After binding to auxin, it interacts with AUX/IAA proteins, activating their ubiquitination. The degradation of the Aux/IAA proteins by the 26S proteasome releases Auxin Response Factors (ARF) from their repression, activating the expression of auxin-responsive genes in the plant (Leyser, 2018). For this reason, the search for new natural compounds that can replace or complement the existing synthetic auxinic herbicides is essential for diversifying the range of herbicides. In fact, Graña et al. (2017), showed the ability of scopoletin, a plant natural compound belonging to the group of coumarins, to fit into the auxin-binding site TIR1 (Transport Inhibitor Response 1) at the same place as auxin and competing with this hormone for the TIR1 receptor, which compromised root development by inducing wrong microtubule assembling, mitochondrial membrane depolarization and ultimately cell death, in a similar way to auxin herbicides. On the other hand, several studies about specialized metabolites found that alterations in root meristem organisation and root morphology are mainly guided by alterations at the auxin polar transport within the root (Araniti et al., 2017; López-González et al., 2020). Polar auxin transport is a specialized mechanism governing asymmetric auxin distribution in plants, allowing the movement of IAA from shoot sources to root sink tissues (Rashotte et al., 2000). Auxin polar transport primarily relies on membrane transporters, including influx carriers like AUX1/LAX and efflux transporters represented by PINFORMED (PIN) and ATP-binding cassette subfamily B (ABCB) proteins (Balzan et al., 2014). The main auxin inhibitors include Naphthylphthalamic Acid (NPA) and *p*-chlorophenoxyisobutyric acid (PCIB), among others (Oono et al., 2003; Abas et al., 2021) (Fig. S1). Each of these inhibitors operates through distinct modes of action to interfere with auxin-related processes within plants, ultimately leading to significant effects on growth and development. PCIB interferes with the enzymatic conversion of tryptophan to indole-3-acetic acid (IAA), a key step in auxin biosynthesis (Fig. S1). By inhibiting this conversion, PCIB reduces the levels of active auxin in the plant, disrupting auxin-mediated processes like cell elongation and root growth (Oono et al., 2003). On the contrary, NPA is a competitive inhibitor of auxin transport proteins. By blocking the action of PIN proteins, NPA prevents the polar transport of auxins, disrupting their distribution within the plant (Abas et al., 2021).

Concerning the specialized metabolites important in plant defence and adaptation, azelaic acid (AZA) (or nonanedioic acid) plays a pivotal role. This saturated dicarboxylic acid (Fig. S1), produced either by plants (rice, wheat, barley, among others), fungi and a smaller amount by human metabolism (Sharma et al., 2020), has gained attention in the last years due to its versatile properties and potential applications in medicine and pharmacology (Searle et al., 2022). Moreover, this compound plays an important role in plant defence and resistance to biotic stress. In particular, Jung et al. (2009) reported that AZA accumulation in *Arabidopsis* was related to systemic defence responses against bacterial infections, demonstrating that both the azelaic acid and the *AZELAIC ACID INDUCED 1 (AZI1)* gene took action in priming defences of the plant, being part of systemic immunity. Cecchini et al. (2019) reported that *Arabidopsis* plants treated with AZA showed increased resistance to *Pseudomonas syringae* infection by inducing systemic resistance and that azelaic acid caused root growth inhibition when directly applied to the roots. In addition, the allelopathic activity of AZA has already been demonstrated as the main allelopathic constituent of aqueous extracts of *Jatropha curcas,* showing strong inhibitory activity on *Zea mays* seedlings (Ma et al., 2011). Andriana et al. (2018) also identified azelaic acid as one of the chemical components isolated from the extract of the weed *Tridax procumbens*, which has been shown to have potent allelopathic activity. The variety of biological activities shown by AZA, the possibility to be synthesized in an inexpensive and easy way [it is synthetically obtained with pelargonic acid by ozonolysis of oleic acid (Brenna et al., 2020)], and its low toxicity against mammals (LD_{50} < 2000 mg/kg), makes AZA an extremely interesting candidate for the research of botanical-based bioherbicides. Therefore, the study aimed to *in-vitro* evaluate the phytotoxic potential of AZA on the model species *Arabidopsis thaliana* to identify the main mechanism/s of action of the compound in the plant metabolism and its key biologically active concentration. Since the preliminary results suggested that the root is the main target organ of this molecule, this study was focused on the investigation of the potential mode of action of AZA on the roots by using an integrated approach (cyto-morphological, transgenic, pharmacological, spectrophotometric, and molecular docking).

2. Materials and methods

2.1. Plant material and dose-response curve

Arabidopsis thaliana (L.) Heynh. ecotype Columbia (Col-0) seeds were sterilized and vernalized, as previously reported by Díaz-Tielas et al. (2012). Seeds were sown on square Petri dishes containing plant agar supplemented with 0.44% Murashige-Skoog nutrients (Sigma-Aldrich, Saint Louis, USA) and 1% sucrose. Azelaic acid (nonanedioic acid, Sigma-Aldrich, Darmstadt, Germany) was diluted in ethanol (EtOH) (0.01%) and added to growth agar solution to reach the following concentrations: 0, 12.5, 25, 50, 75, and 150 μM.

Twenty-four seeds were sown on each square dish, with five replicates per treatment. Plates were vertically placed in a growth chamber with the following photoperiod: 16 h light (120 μmol m^{-2} s^{-1})/8 h darkness, 22 ± 2 °C and 55% relative humidity. After 14 days of growth, *A. thaliana* primary root length was measured to obtain a dose-response curve. At the end of the experiment, plates were scanned for measuring lateral root length (LRL), lateral root number (LRN), lateral root density (LRD), adventitious root length (ARL), adventitious root number (ARN) and adventitious root density (ARD) by using the software Image Pro-Plus 6.0 (Media Cybernetics, Silver Spring, MD, USA).

2.2. Root apical meristem (RAM) analysis

The propidium iodide staining (mPS-PI Staining) was used to analyse the root apical meristem (RAM) on *A. thaliana* seedlings grown in the presence of IC_0 and IC_{50} (44 μM) azelaic acid for 7 days. The experiments were carried out following the protocol proposed by Truernit et al. (2008), and modified by Sánchez-Moreiras et al. (2018). After staining, seedlings were visualised using a Leica TCS SP5 microscope (Wetzlar, Germany) with an excitation wavelength of 543 nm and an emission of 576–712 nm. Then, the following parameters were quantified according to Bruno et al. (2021): (*i*) meristem cell number (MCN), expressed in arbitrary units and calculated as the cell number from the quiescent center (QC) to the first elongated cortex cell at precortex layer level; (*ii*) meristem zone length (MZL), expressed in μm and estimated as the length from QC to the first elongated cortex cell; (*iii*) meristem zone width (MZW), expressed in μm and considered as the distance between the two opposite cortex cells; (*iv*) columella width (CW) and (*v*) columella length (CL), expressed in μm and measured from the QC level to the lateral or the end of the columella, respectively; (*vi*) columella area, expressed in μm^2 and represented as the total area with cells having starch granules; (*vii*) cell length and (*viii*) cell width of protodermal, precortical and proendodermal cells, expressed in μm. All parameters were calculated with the Image Pro-Plus 6.0 software (Media Cybernetics, Silver Spring, MD, USA).

2.3. Root ultra-structural analysis and starch staining

For Transmission Electron Microscopic (TEM) analysis, *A. thaliana* seedlings were grown for 7 and 14 days in the presence of IC_0 and IC_{50} (44 μM) azelaic acid. Then, radicle tips (1–2 mm) were cut, and the technical procedure was performed as already reported by Álvarez-Rodríguez et al. (2022). The meristem root longitudinal sections were visualised using the JEOL JEM-1010 (80kv) TEM equipped with a CCD Orius and Digital Montage Plug-in camera (Gatan Inc., Gatan, CA, USA) and Gatan Digital Micrograph software (Gatan Inc.).

For starch staining, roots grown for 7 days in IC_0 and IC_{50} (44 μM) azelaic acid were immersed in Lugol staining solution (10%) for 5 min. Then, three roots per treatment were visualised using a Nikon Eclipse 800 optical microscope equipped with a Sight Nikon DS-U2 digital camera and NIS-Elements D 2.30 SP1 software. The Integrated Optical Density (IOD) was quantified using Image-Pro Plus 6.0 (Media Cybernetics, Silver Spring, MD, USA).

2.4. GC-MS-driven IAA quantification and bioassays with GFP transgenic lines

The quantification of indole-3-acetic acid (IAA) was conducted in accordance with a method originally proposed by Rawlinson et al. (2015) and modified by Landi et al. (2020). Concerning GFP bioassay, *Arabidopsis* seeds belonging to diverse green fluorescent protein (GPF) transgenic lines related to auxin content *pDR5::GFP* (Bruno et al., 2021), or auxin transport proteins *pPIN1::GFP, pPIN2::GFP, pPIN3::GFP, pPIN4::GFP* and *pPIN7::GFP* (Araniti et al., 2017) were used in this study. Azelaic acid-treated (44 μM) and untreated (0 μM) seedlings were analysed after 7 days of growth. RAMs were visualised under a Leica TCS SP5 microscope (Wetzlar, Germany) with 488 and 500–540 nm excitation and emission wavelengths, respectively. The Corrected Total Cell Fluorescence signal was calculated with the ImageJ software according to the following equation:

CTCF = Integrated Density – (Area of Selected Cell x Mean Fluorescence of Background readings).

2.5. Auxin reversion bioassay using p-chlorophenoxyisobutyric acid (PCIB)

To evaluate the possible auxin implication in the mode of action of azelaic acid, *A. thaliana* seedlings were grown for 7 days with IC_0, IC_{50} (44 μM) or IC_{80} (76 μM) azelaic acid, 15 μM *p*-chlorophenoxyisobutyric acid (PCIB) (Sigma-Aldrich), and a combination of 15 μM PCIB plus IC_{50} or IC_{80} azelaic acid (Oono et al., 2003). Then, phenotypical effects were *de visu* analysed using a stereo-microscope Nikon SMZ 1500.

2.6. Root gravitropism analysis

To evaluate the ability of the roots to response to gravitropic stimulus, *A. thaliana* seedlings were grown for 6 days in agar medium and then transplanted to a new agar medium containing IC_0 or IC_{50} azelaic acid. Petri dishes were then rotated 90° to analyse the gravistimulation of the roots. Evolution on the root curvature was monitored at 0, 3, 6 and 12 h, and the curvature angles on root reorientation were measured using the Image Pro-Plus 6.0 software (Media Cybernetics, Silver Spring, MD, USA).

2.7. Molecular docking simulation

Molecular docking was computationally simulated using ICM-Pro software (version 3.9-3, Molsoft). The 3D structure of *Arabidopsis thaliana* TIR1 (Transport Inhibitor Response 1) was downloaded from the protein data bank (RCSB PDB, https://www.rcsb.org/; accession code: 2p1q; resolution, R = 1.91 Å). To retrieve the receptor, the non-protein structures (2-(1H-indole-3-yl) acetic acid (IAA), inositol hexakisphosphate (InsP6) and IAA/peptide), as well as the water molecules of the crystal structure, were removed. Subsequently, according to the default ICM-Pro procedures (Abagyan and Totrov, 1994), the orientation of His, Pro, Asn, Gln, and Cys residues was optimized, missing heavy atoms were constructed, and hydrogen atoms were optimized. The structure of azelaic acid (AZA) (accession code: 2266) was downloaded from NCBI PubChem (https://pubchem.ncbi.nlm.nih.gov/). The 2D structure was converted to 3D, additional hydrogen atoms were added, and the 3D geometries were optimized using the MMFF force field implemented in ICM-Pro. The lowest energy conformations were used as initial geometries for the molecular docking simulations. Blind flexible docking was simulated to optimize the internal coordinates of azelaic acid located at the protein binding site. The AZA-TIR1 complex was evaluated and classified based on full ICM scoring functions. A low ICM score suggests favourable ligand-protein binding affinity.

2.8. Statistical analysis

All the experiments were carried out using a completely randomised design with different number of replicates depending on the experiment: root morphology measurements, PCIB reversion bioassay and gravitropic response experiment were done using ten replications; RAM analyses were performed using five replications; GFP experiments were done using four replications, and auxin content, TEM and Lugol staining were performed using three replicates. Confocal and RAM analyses were repeated three times with similar results. Non-linear regression was used to fit data from dose-response curves (expressing control average growth as 100%) to calculate IC_{50} and IC_{80} as the two key concentrations for root length inhibition (azelaic acid doses needed for the 50% and 80% of primary root length inhibition, respectively).

First, all data were checked with an exploratory analysis to detect *outliers*. Then, the Kolmogorov-Smirnov test was carried out to check the normality of the data and the Levene test was used to test the homogeneity. Considering this, data from morphology measures were analysed through Kruskal-Wallis ($p \leq 0.05$). In this case, different letters refer to significant differences among treatments. By contrast, gravitropism experiment, RAM analyses, CTCF quantification in GFP experiments, GC-MS auxin quantification and IOD quantification in Lugol staining were analysed through *t*-test. All data were analysed using IBM SPSS Statistics v. 25.0 software (SPSS, Chicago).

3. Results

3.1. Effects of azelaic acid on root morphology and RAM

The dose-response curve performed on *A. thaliana* showed the strong phytotoxic potential of azelaic acid. The results highlighted that AZA was active already at concentrations as low as 25 μM, causing a 20% reduction in primary root growth. The inhibition of primary root growth increased with increasing AZA concentrations, reaching 80% inhibition at 75 μM. The non-linear regression fitting of the dose-response curve ($R^2 = 0.916$) allowed us to identify the IC_{50} and IC_{80} values for Primary Root Length (PRL), which were 44 and 76 μM, respectively (Fig. 1d). IC_{50} concentration (44 μM) was successively used as the key concentration for the study of the AZA mode of action. As shown in Fig. 1a, while control seedlings showed uniform morphology and development, AZA-treated seedlings (IC_{50} and IC_{80}, Fig. 1b and c, respectively) showed strong morphological and growth alterations. Azelaic acid induced an increment of both adventitious and lateral root densities in *A. thaliana* seedlings while reducing primary root growth compared to the control (Fig. 1g and j). Although Lateral Root Length (LRL) and Lateral Root Number (LRN) increased for the lowest concentration tested, increasing AZA concentrations caused a generalized decrease in both LRL and LRN,

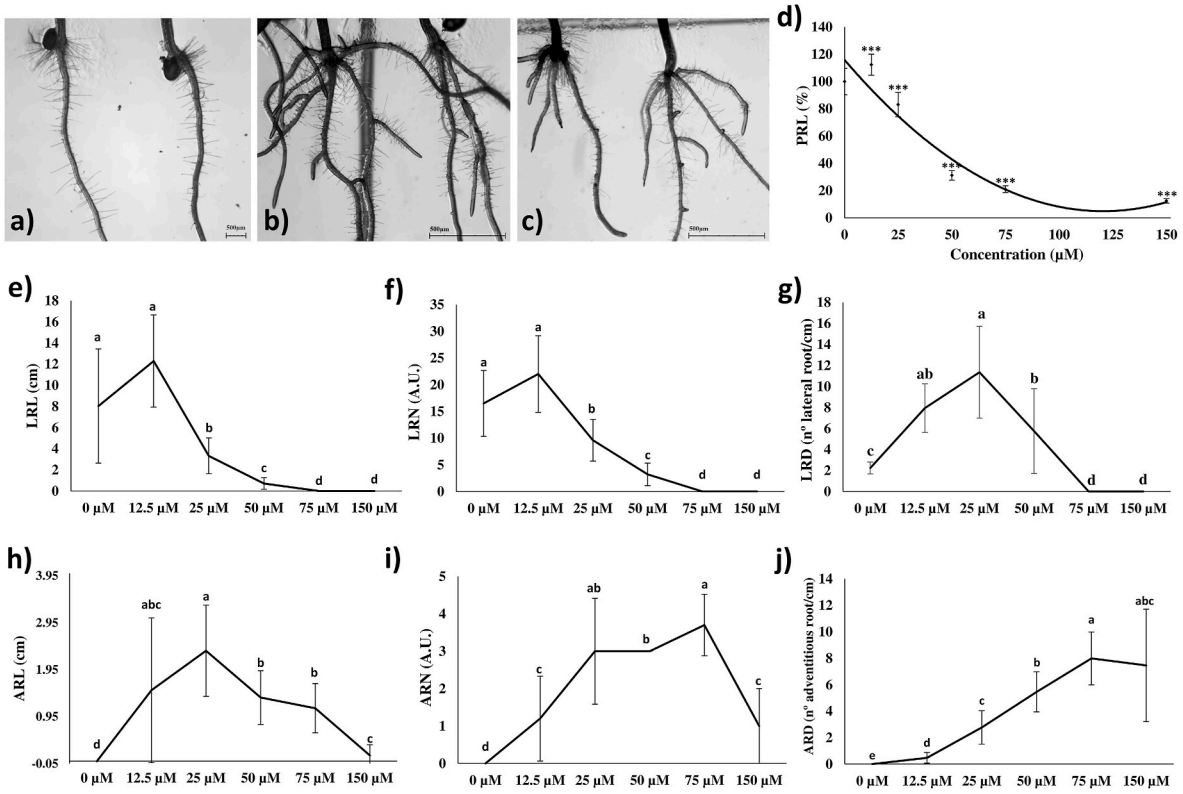

Fig. 1. Effects of azelaic acid on root morphology of *Arabidopsis thaliana* after 14 days of growth. **a)** Untreated roots; **b)** Azelaic acid-treated roots with the IC_{50} concentration (44 μM); **c)** Azelaic acid-treated roots with the IC_{80} concentration – 76 μM; **d)** Dose-response curve of the Primary Root Length (PRL) of *A. thaliana* seedlings, expressed in percentage of the control root growth ($R^2 = 0.916$ and non-linear regression formula $y = 0.0076x^2 - 1.8408x + 115.95$). Asterisks indicate differences compared to control root growth; **e)** Lateral Root Length (LRL), expressed in cm; **f)** Lateral Root Number (LRN), expressed in arbitrary units; **g)** Lateral Root Density (LRD), expressed in number of lateral roots/cm; **h)** Adventitious Roots Length (ARL), expressed in cm; **i)** Adventitious Roots Number (ARN), expressed in arbitrary units; **j)** Adventitious Roots Density (ARD), expressed in number of adventitious roots/cm. Data were statistically analysed through Kruskal-Wallis with $p \leq 0.05$. Different letters indicate significant differences between treatments. N = 10.

inducing a completely lateral root inhibition for the highest concentrations assayed (75 and 150 μM) (Fig. 1e and f, respectively). By contrast, Lateral Root Density (LRD) increased with increasing AZA concentrations, except for the highest concentrations assayed (75 and 150 μM) since any root development was completely inhibited by this strong treatment (Fig. 1g). In addition, Adventitious Root Number (ARN) and Adventitious Root Density (ARD) experienced an upward trend since higher adventitious root production was observed with increasing AZA concentrations (Fig. 1i and j). The Adventitious Root Length (ARL) trend was almost equal, reaching a maximum at 25 μM and decreasing with increasing AZA treatments until the strongest assayed concentration (Fig. 1h).

After 7 days of treatment, azelaic acid significantly altered the root apical meristem (RAM) of *A. thaliana* seedlings (Figs. 2 and 3). AZA treatment caused apical meristem reduction and shortening of the distal and proximal meristem (DM and PM), inducing advancement of transition and elongation zones (TZ and EZ), which appeared earlier than in control due to a lower number of apical meristematic cells. Moreover, AZA treatment induced elongation and narrowing of the meristematic cells, leading to thinner and weaker roots (Fig. 2b). In fact, AZA-treated roots showed a reduction in MCN (70% lower than control roots), in MZL (50% lower than control), and also in MZW (42% lower than control), as shown in Fig. 3a, b and 3c, respectively. In addition, columella was also affected by azelaic acid since CW and CL were significantly decreased compared to control roots (both with a 15% reduction). In comparison, CA was 11% lower than the control (Fig. 3d, e and 3f, respectively). The data demonstrated that AZA induced shortening of the meristematic zone (50% lower than control), altering both the organisation and shape of protodermis, precortex and proendodermis

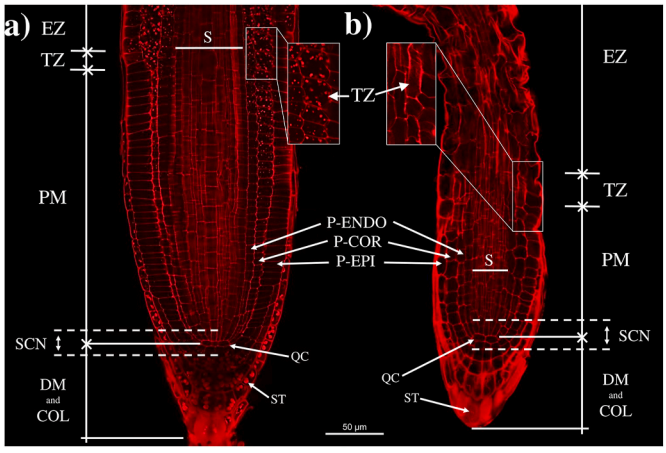

Fig. 2. Confocal microscope images of 7 days-old seedlings of *Arabidopsis thaliana* untreated **(a)** and treated with IC_{50} (44 μM) azelaic acid **(b)** after being stained with propidium iodide. Root apical meristem (RAM) zones are marked: elongation zone (EZ), transition zone (TZ), proximal meristem (PM), distal meristem (DM), stem cell niche (SCN), stele (S), columella (COL), protodermis (P-EPI), precortex (P-COR) and proteondodermis (P-ENDO). In addition, in RAM, the quiescent center (QC) and statoliths (ST) can be observed. This experiment was repeated three times with similar results. Scale bar: 50 μm. N = 5.

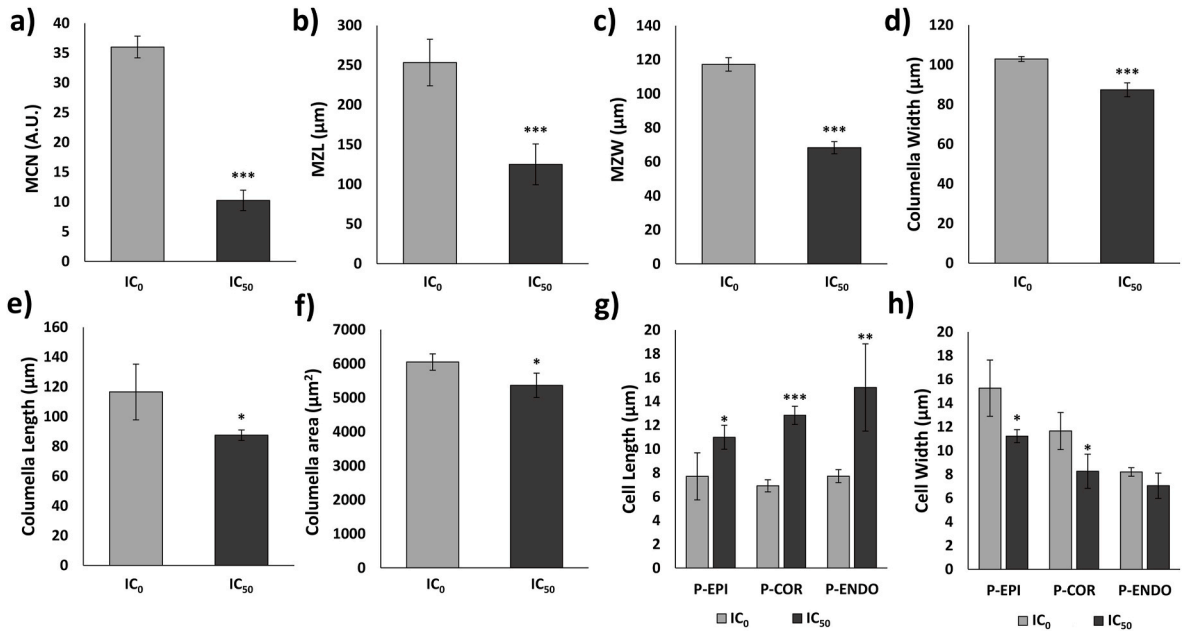

Fig. 3. Root apical meristem (RAM) morphology measurements of 7 days-old *A. thaliana* seedlings treated with IC_0 (control) and IC_{50} (44 μM) azelaic acid. **a)** MCN (meristem cell number, expressed in arbitrary units); **b)** MZL (meristem zone length, expressed in μm); **c)** MZW (meristem zone width, expressed in μm); **d)** columella width (CW) (expressed in μm); **e)** columella length (CL) (expressed in μm); **f)** columella area (expressed in μm^2); **g)** cell length (expressed in μm); **h)** cell width (expressed in μm). Data are represented as mean ± standard deviation (SD) (IC_0: control; IC_{50}: 44 μM azelaic acid). Statistical differences were estimated through Student's *t*-test with * $p \leq 0.05$, ** $p \leq 0.01$ or *** $p \leq 0.001$. N = 5.

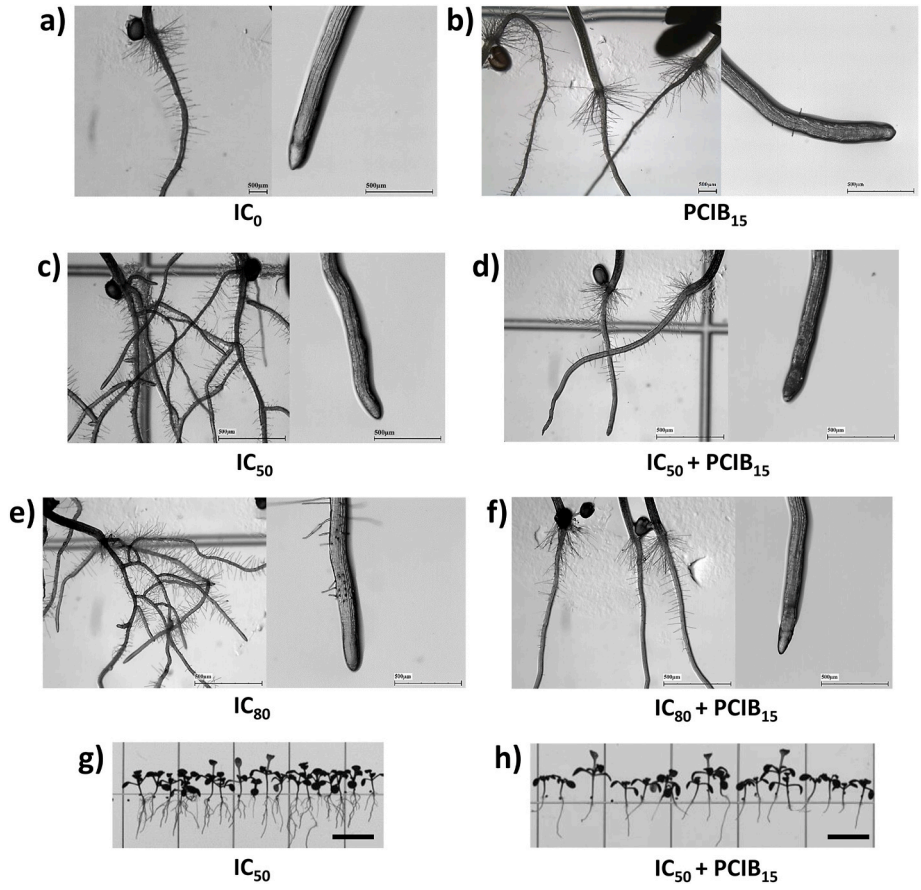

Fig. 4. *Arabidopsis thaliana* seedling roots treated with IC_0 (control) **(a)**, PCIB (15 μM) **(b)**, IC_{50} (44 μM) azelaic acid **(c, g)**, IC_{50} azelaic acid + PCIB **(d, h)**, IC_{80} azelaic acid (76 μM) **(e)** and IC_{80} azelaic acid + PCIB **(f)** observed under stereo-microscope after 14 days of growth. Scale bars (a–f) 500 μm, (g, h) 1 cm. N = 10.

layer cells (Fig. 3g and h), which were larger after AZA treatment (30%, 46% and 49% larger than the control, respectively). Moreover, protodermis and precortex cells reduced their width compared to control cells (36% and 40% thinner than the control; Fig. 3g and h, respectively). This confirmed that root apical meristem cells of treated roots, although fewer, were longer and thinner due to AZA treatment.

3.2. Influence of p-chlorophenoxyisobutyric acid (PCIB) on root growth and development of azelaic-treated plants

Based on azelaic acid morphological effects on *A. thaliana* seedlings, such as lateral and adventitious root stimulation, a reversion bioassay using the auxin inhibitor PCIB was done to clarify the possible auxin implication on the mode of action of azelaic acid. After 14 days of growth, control seedlings experienced uniform growth (Fig. 4a), as well as those control plants treated with the anti-auxinic PCIB (15 μM) (Fig. 4b). In contrast, seedlings treated with AZA (IC_{50}) experienced a significant appearance of adventitious and lateral roots along the whole root (Fig. 4c and g), as previously observed in the morphological bioassay. The same effects were also visualised in IC_{80} AZA-treated seedlings (Fig. 4e). However, the phenotype of seedlings grown in agar medium supplemented with IC_{50} AZA + PCIB showed a completely different morphology than those treated only with AZA (Fig. 4d and h), as the anti-auxinic PCIB reversed AZA-induced morphological

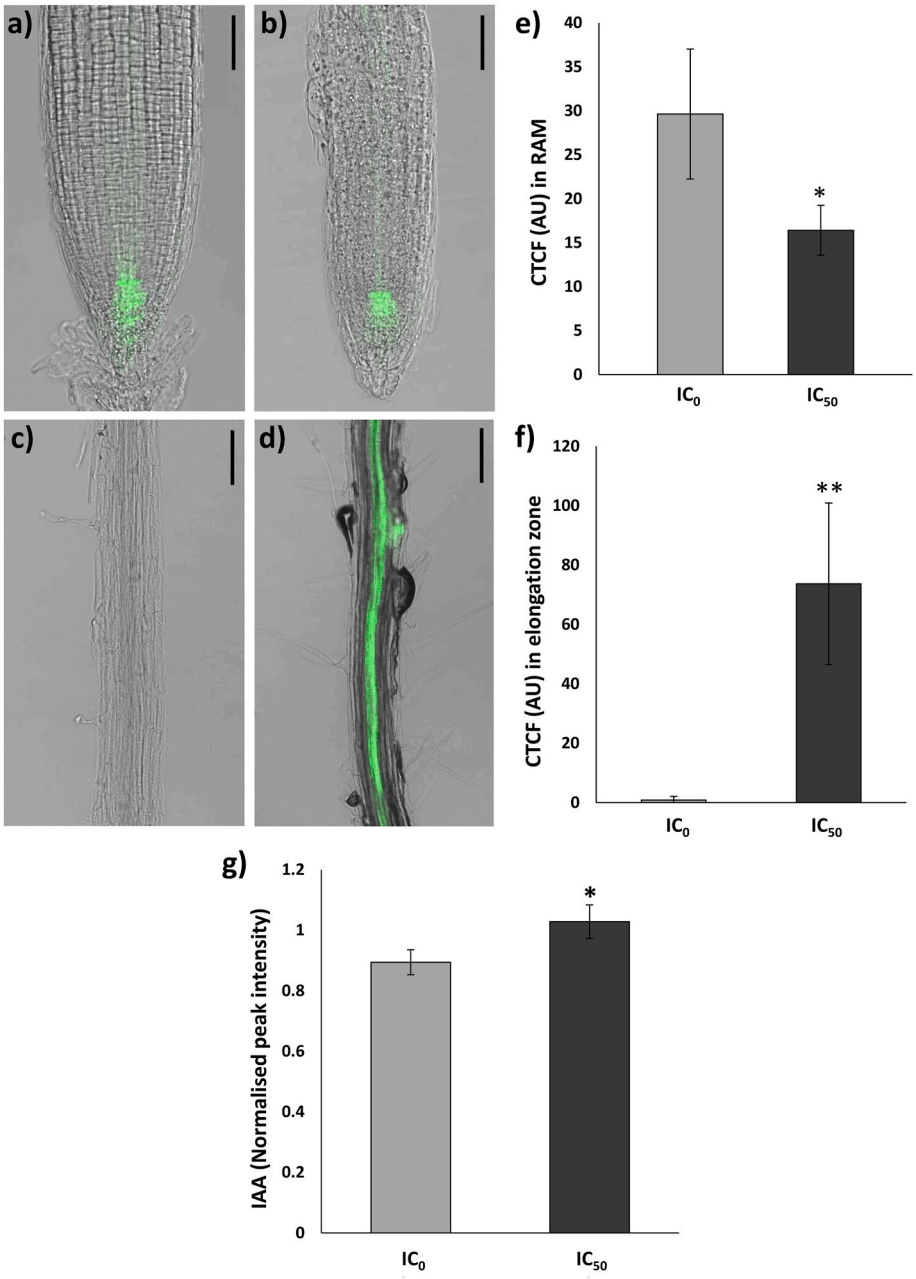

Fig. 5. Confocal microscopy images of 7 days-old *Arabidopsis thaliana pDR5::GFP* transgenic line seedlings. Root apical meristem (RAM) of untreated **(a)** and treated seedlings with IC_{50} (44 μM) azelaic acid **(b)**. Root elongation zone of untreated **(c)** and treated seedlings with IC_{50} azelaic acid **(d)**. Corrected Total Cell Fluorescence (CTCF) is expressed as arbitrary units (AU) of fluorescence intensity measured in the RAM **(c)** and in the elongation zone **(f)**. Quantification of indole-3-acetic acid (IAA) in *Arabidopsis thaliana* untreated and treated seedlings with IC_{50} (44 μM) azelaic acid **(g)**. Data are represented as mean ± standard deviation (SD) (IC_0: control; IC_{50}: 44 μM azelaic acid). This experiment was repeated three times with similar results. Statistical differences were estimated through Student's *t*-test with * $p \leq 0.05$, ** $p \leq 0.01$ or *** $p \leq 0.001$. Asterisks indicate significant differences compared to control roots. Scale bars 100 μm. N = 4.

alterations, such as adventitious and lateral roots overproduction, resulting in roots with a phenotype similar to control phenotype (Fig. 4h). Indeed, this reversion was also effective with IC_{80} AZA + PCIB (Fig. 4f).

3.3. Effects of azelaic acid on auxin content and its polar transport (PIN proteins) and distribution

A spectrophotometric and transgenic approach was used to monitor auxin quantity and distribution, by visualising the auxin sensor (*DR5::GFP*) and the efflux transporter proteins (*PIN1*, *PIN2*, *PIN3*, *PIN4* and *PIN7*) under confocal microscopy.

Regarding the signal of auxin content and distribution, the *pDR5*-dependent GFP fluorescence of control roots showed the typical maximum fluorescence in the root tip and procambium cells (Fig. 5a). However, AZA-treated roots experienced a significant reduction in GFP signal intensity (≈45% lower than the control) in the root tip and procambium cells (Fig. 5b and e). On the contrary, a significant accumulation of GFP fluorescence signal was detected in the elongation zone and throughout the entire root of AZA-treated seedlings (85-fold higher than the control) (Fig. 5d–f), while this GFP signal was almost absent in the elongation zone of control roots (Fig. 5c). In addition, the GC-MS-driven auxin quantification showed a significant increment of total auxin content of 15% in plants treated with azelaic acid (Fig. 5g). Both signal intensity and distribution of the five PIN proteins tested in this study were strongly altered and inhibited (Fig. 6), with values of

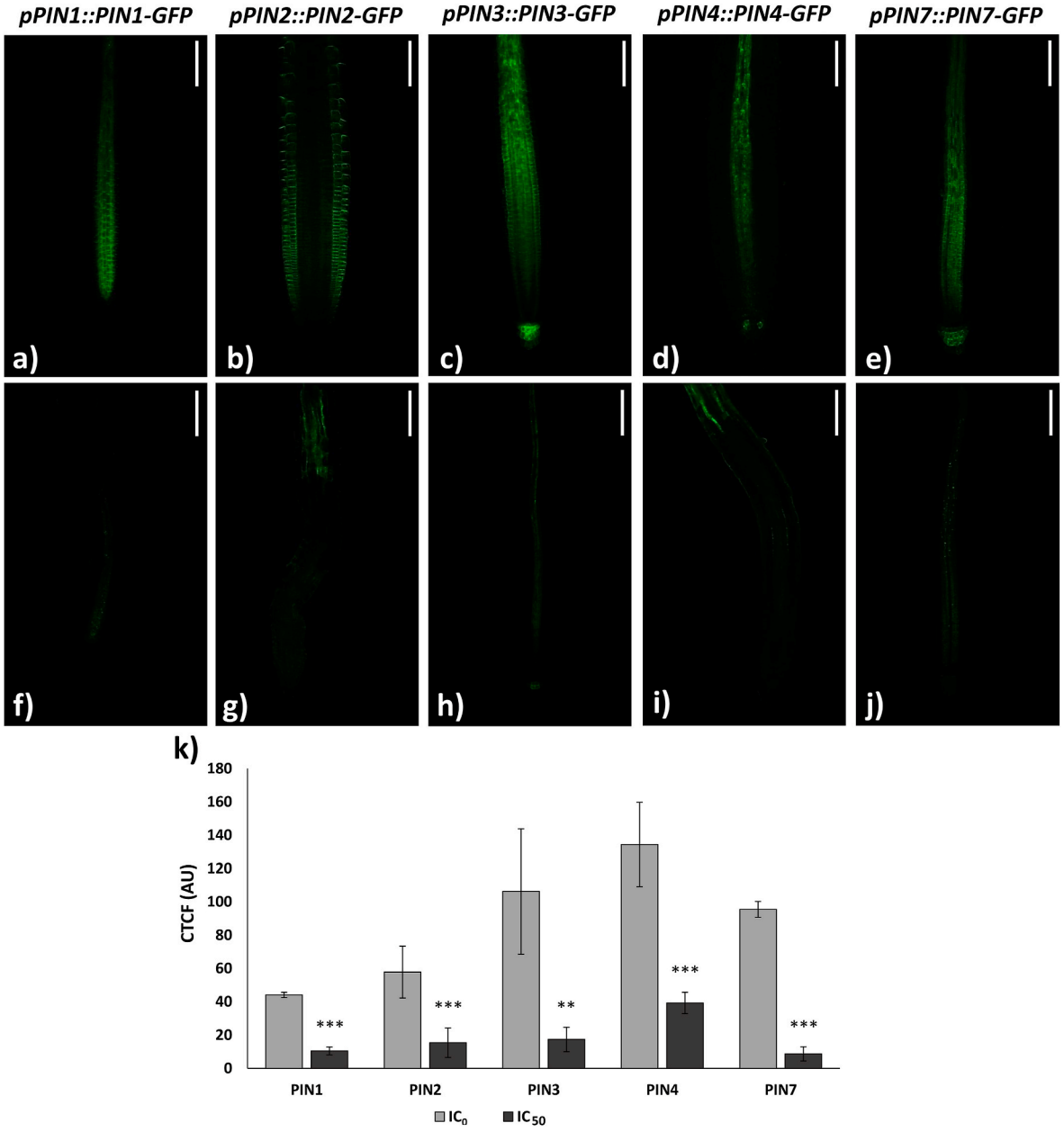

Fig. 6. Confocal laser images of primary root tips of the following *Arabidopsis thaliana* transgenic lines*: pPIN1::PIN1-GFP, pPIN2::PIN2-GFP, pPIN3::PIN3-GFP, pPIN4::PIN4-GFP* and *pPIN7::PIN7-GFP* treated with IC_0 (**a**, **b**, **c**, **d**, and **e**, respectively) and IC_{50} (44 μM) azelaic acid (**f**, **g**, **h**, **i** and **j**, respectively) for 7 days. Corrected total cell fluorescence (CTCF) of untreated and treated seedlings with IC_{50} (44 μM) azelaic acid **(k)**. The CTCF is expressed in arbitrary units (AU) of fluorescence intensity. Data are represented as mean ± standard deviation (SD) (IC_0: control; IC_{50}: 44 μM azelaic acid). This experiment was repeated three times with similar results. Statistical differences were estimated through Student's *t*-test with * $p \leq 0.05$, ** $p \leq 0.01$ or *** $p \leq 0.001$. Asterisks indicate significant differences compared to control roots. Scale bars 100 μm. N = 4.

Corrected Total Cell Fluorescence (CTCF) that were notably reduced in AZA roots compared to control roots (Fig. 6k). Concerning PIN1 and PIN3 distribution, the GFP intensity significantly decreased along the RAM in a 77% and 84%, respectively, compared to control roots (Fig. 6f, h, 6k). Regarding PIN2 and PIN4, these two mutants showed a similar pattern to PIN1 results since the global GFP fluorescence of RAM was reduced by 74% and 71%, respectively, after AZA treatment (Fig. 6g, i, 6k). Finally, the GFP signal in PIN7 GFP mutants was remarkably inhibited, being 92% lower than the control (Fig. 6j and k).

3.4. Ultra-structural and gravitropic root response of *Arabidopsis thaliana* roots after azelaic acid treatment

Monitorization of the gravitropic response was performed to measure the plants' ability to effectively respond to gravitropism by evaluating the curvature angle of the root apex after a rotation of 90°. The results showed that AZA affected the ability of the root to respond to the gravitropic stimulus by slowing down the curvature of the root apex over time (Fig. 7). In control roots, the gravitropic curvature of the root apex reached 90° already 9 h after rotation whereas those AZA-treated

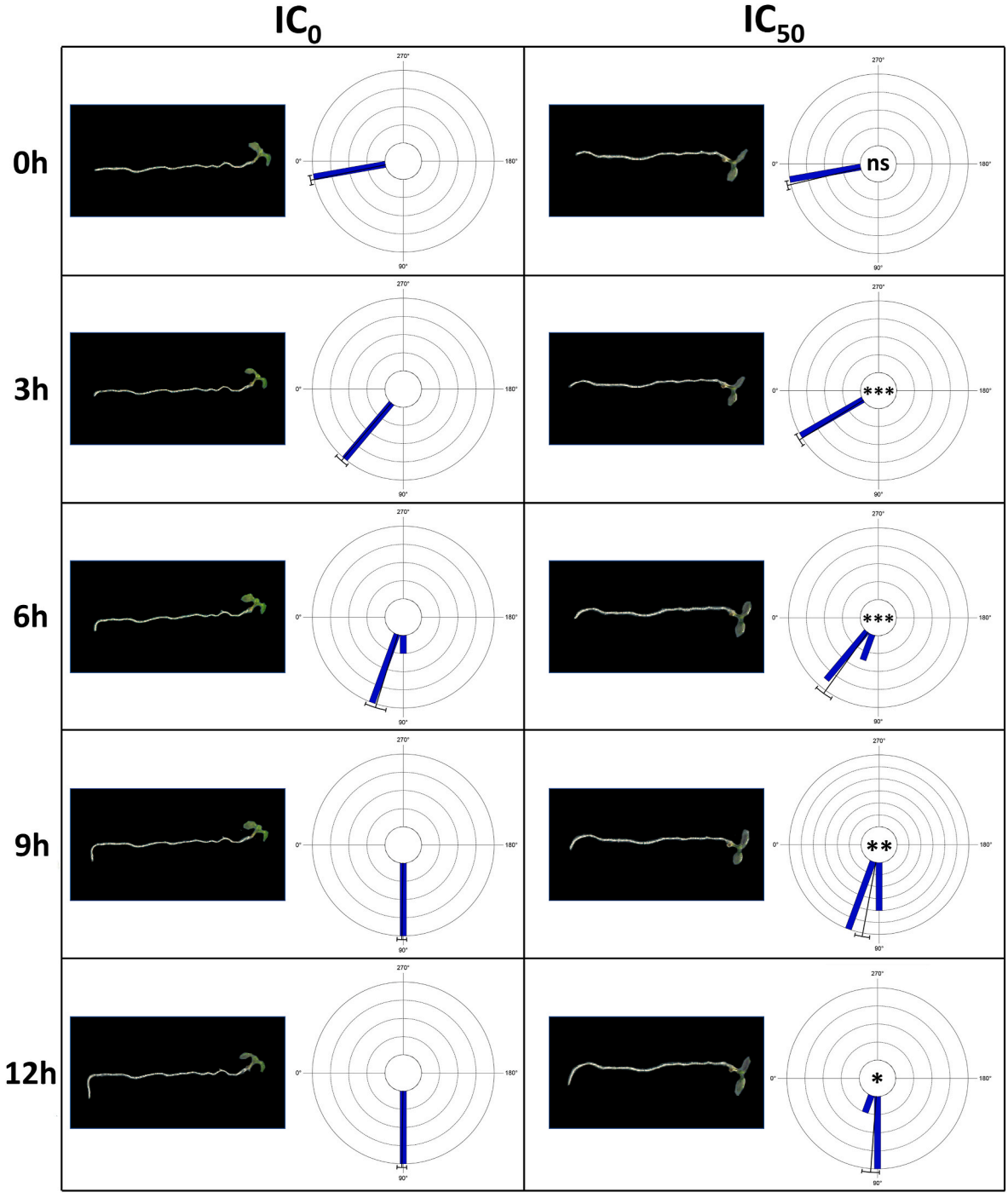

Fig. 7. Azelaic acid effects on the time-course gravitropic response of *Arabidopsis thaliana* roots. Plants were rotated 90° and root apex curvature was monitored after 0, 3, 6, 9 and 12 h. Circular diagrams express the angle curvature of the root apex, where blue bars represent data tendency and black bars represent standard deviation (IC_0: control; IC_{50}: 44 μM azelaic acid). Data were analysed through Student's *t*-test with * $p \leq 0.05$, ** $p \leq 0.01$ or *** $p \leq 0.001$. Asterisks inside the circular diagrams indicate significant differences compared to control roots at each measured time; ns means no statistical differences. N = 10.

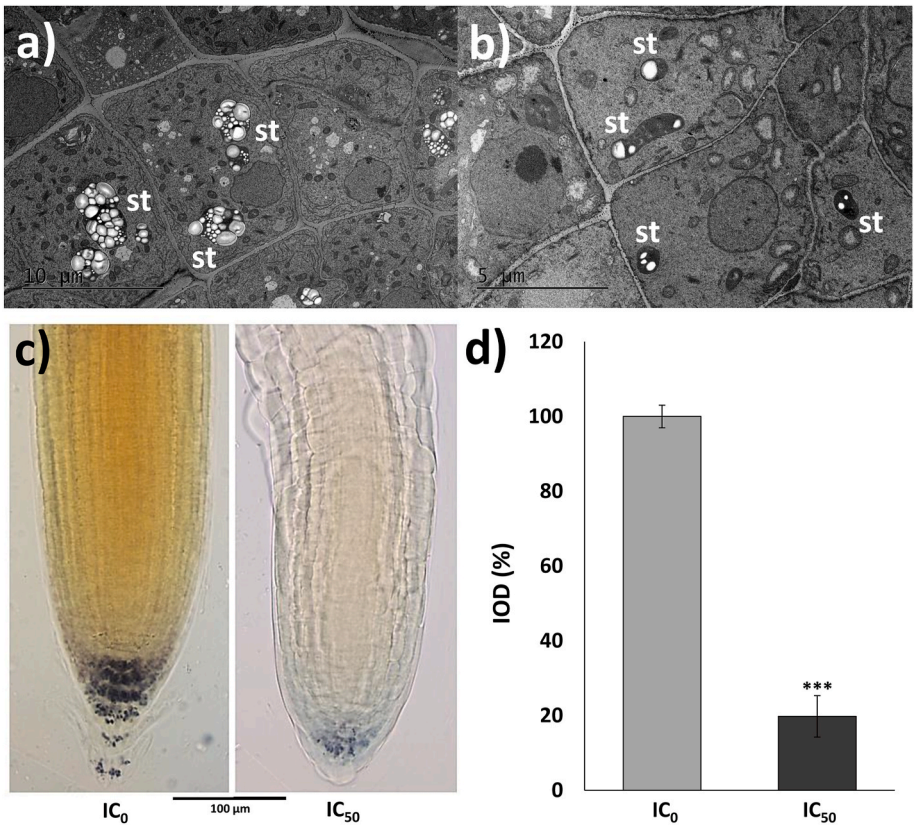

Fig. 8. Transmission electron microscopy images of untreated **(a)** and IC_{50} (44 µM) azelaic-treated *Arabidopsis thaliana* roots **(b)** after 7 days of growth (st: statoliths). Scale bars: 10 and 5 µm, respectively. Optical microscopy images of control **(c-left)** and IC_{50} azelaic-treated roots **(c-right)** stained with Lugol after 7 days of growth. Scale bar: 100 µm. Integrated Optical Density (IOD) was quantified for untreated and treated roots after the Lugol staining **(d)**. IOD is expressed in the percentage of the control. Data are represented as mean ± standard deviation (SD) (IC_0: control; IC_{50}: 44 µM azelaic acid). Statistical differences were estimated through Student's *t*-test with * $p \leq 0.05$, ** $p \leq 0.01$ or *** $p \leq 0.001$. N = 3.

seedlings needed 12 h to achieve a curvature close to 90°.

TEM images showed a reduction in statoliths density in the columella of AZA-treated roots compared with control roots (Fig. 8a and b). This observed reduction in the starch organelles was confirmed by the starch-specific Lugol staining and its subsequent quantification of the Integrated Optical Intensity (IOD), as the IOD of the AZA-treated roots was five-times lower than in control roots (Fig. 8c and d).

3.5. Computational simulation with azelaic acid on TIR1

Based on the results of previous experiments and the auxin imbalance observed after AZA treatment, computational simulations were performed to evaluate the possible involvement of TIR1 (Transport Inhibitor Response 1), a protein that functions as an auxin receptor in *Arabidopsis thaliana*, in the mode of action of azelaic acid.

Molecular docking strategy revealed that the ligand was buried in the auxin pocket of the receptor (Fig. 9). A low docking score value (−27.67), as well as the low RTCNN (Neural Network Score) score value (−18.03) of the ligand-receptor complex, supported this hypothesis. The lower the docking score and the RTCNN score are, the better the predicted ligand-receptor interaction. This suggests that the ligand has a high affinity for this site and could modulate the receptor activity. At

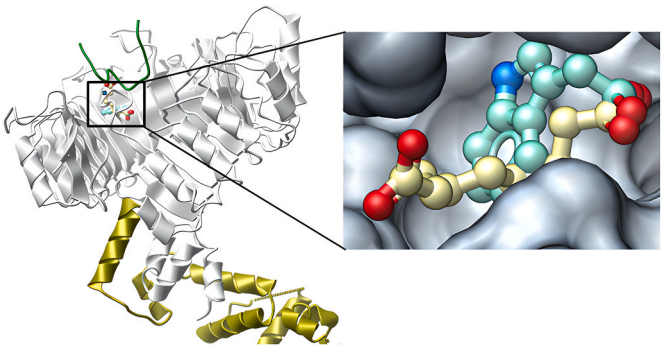

Fig. 9. Analysis of the azelaic acid binding site in molecular docking ICM-Pro using the crystal structure of TIR1 as a receptor (PDB:2P1Q). The structures of azelaic acid (yellow) and indoleacetic acid (blue) in the TIR1 pocket are zoomed in the right part of the image.

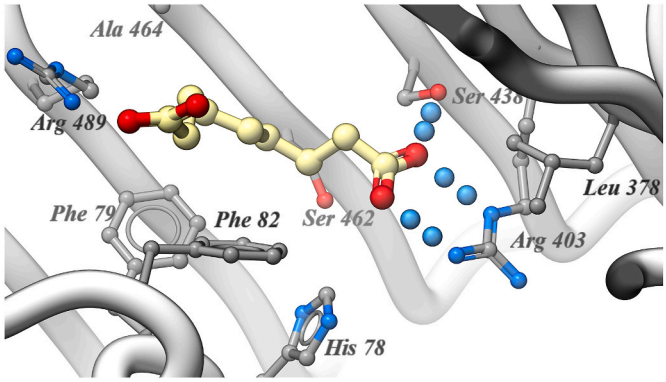

Fig. 10. Hot residues of the AZA-TIR1 complex in the binding pocket. The ligand is colored in yellow and the hydrogen bonds are shown as blue dots. AZA: azelaic acid; TIR1: Transport Inhibitor Response 1.

this binding site, azelaic acid established hydrophobic interactions with residues Phe82, Phe79, His78, Ala464 and Leu378, which favours the orientation of the ligand in the auxin pocket (Fig. 10). In addition, carboxylate groups allowed to establish dipole-dipole interactions with polar residues, such as Arg489, and as expected, receptor binding was strengthened through hydrogen bonds of carboxylate groups with Arg403 and Ser438 residues. Computational molecular docking studies showed that azelaic acid binds to TIR1 in the auxin binding pocket and competes for the binding site.

4. Discussion

Based on our results, azelaic acid strongly alters the morphology and anatomy of *A. thaliana* roots, affecting its growth and development. Moreover, AZA showed strong phytotoxic activity, with IC_{50} and IC_{80} values as low as 44 and 76 μM, respectively. These IC values are considered low concentrations in comparison with other plant specialized metabolites with demonstrated phytotoxic activity, such as citral, farnesene, norharmane, etc. (Graña et al., 2013; Araniti et al., 2017; López-González et al., 2020). Azelaic acid caused a significant increment in lateral root density, coinciding with the results obtained by Cecchini et al. (2019), who reported that *Arabidopsis* seedlings grown in the presence of AZA experienced a strong inhibition in primary root growth together with an increment in lateral root density. Moreover, similar alterations were also detected after cadmium short-term exposition of *A. thaliana* seedlings (Araniti et al., 2023). In contrast, azelaic acid induced the appearance of adventitious roots, whose length and density increased with increasing AZA concentrations. Auxin is known to be one of the major endogenous hormones involved in adventitious roots (AR) formation and is considered an effective inducer. Actually, adventitious rooting has been commonly related to auxin stimulation processes since changes in endogenous auxin concentrations are known to affect adventitious root formation (Gonin et al., 2019). Indeed, Huang et al. (2020) reported that exogenous treatment with auxin indole-3-acetic acid induced adventitious root overproduction in *Arabidopsis* plants, while exogenous treatment with naphthylphthalamic acid (NPA), an inhibitor of auxin-polar transport, inhibited adventitious rooting. It has also been demonstrated that *Arabidopsis superroot (sur1)* and *(sur2)* mutants, which overproduce auxin, overproduced AR on the basipetal part of the hypocotyl of *Arabidopsis*, confirming auxin influence on AR formation (Boerjan et al., 1995; Delarue et al., 1998). The morphological alterations obtained after AZA suggest that this molecule could act by inducing auxin imbalance in *Arabidopsis* roots.

In addition, AZA altered the ability of treated roots to react to gravitropic stimulus, slowing down its response in AZA-treated seedlings. A reduction in statolith content in AZA-treated roots was also confirmed after Lugol staining. Zhang et al. (2019) reported that root tips treated with the auxin analogue 1-naphthaleneacetic acid (1-NAA) (Fig. S1) had more starch granule formation by the upregulation of the genes *PGM*, *ADG1*, *SS4*, known for being involved in starch granule synthesis pathways, demonstrating the pivotal role of the local auxin maximum/gradient within the root apex, in the accumulation of starch granules. On the contrary, plants treated with L-kynurenine (L-Kyn), an inhibitor of auxin synthesis, showed less starch granule formation, confirming that auxin within root apex is involved in the accumulation of starch in the columella and, as a consequence, in statolith production (Zhang et al., 2019). Similar results, related to the alteration of auxin transport and statolith formation, were also observed in *Arabidopsis* seedlings exposed to cadmium (Araniti et al., 2023). In particular, plants treated with Cd showed a slower gravitropic response and a reduction of starch granules. The authors suggested a relation between the reduction of starch granules and the lower content of auxin in the RAM (Araniti et al., 2023), which is in concordance with our results. In addition, Zhou et al. (2018) found that exogenous hydrogen peroxide, known to disrupt starch accumulation, led to changes in auxin distribution and reduced root gravitropism in *Arabidopsis* seedlings. Therefore, the reduction in starch granules and the delay of the gravitropic response observed suggest that an alteration in the auxin synthesis or distribution occurs in response to AZA exposition.

All AZA-induced morphological and anatomical alterations suggest that auxin could play a key role in the mode of action of this specialized metabolite. The bioassays with the auxin signal inhibitor PCIB confirmed this hypothesis. As expected, those seedlings grown in the presence of AZA and PCIB did not develop adventitious roots, showing a similar morphology to the control. Similar results were obtained with the natural alkaloid norharmane on *A. thaliana* seedlings. This indole-alkaloid caused adventitious root overproduction, which was reversed after PCIB exposition, suggesting that auxin biosynthesis or polar auxin transport was altered by the treatment with norharmane (López-González et al., 2020).

The auxin-responsive reporter *pDR5::GFP*, which marks auxin signal and distribution along the root, revealed that AZA altered auxin levels and distribution since *pDR5::GFP* fluorescence signal was reduced in the root tip, while significantly increased in elongation and maturation zones. It has been reported that auxin accumulation in the elongation zone and pericycle cells is linked to lateral root formation (Alarcón et al., 2019), which was observed after AZA treatment. De Rybel et al. (2012) obtained that *A. thaliana* roots treated with the molecule naxillin showed stronger DR5 expression than control, specifically in the xylem pole cells adjacent to the root pericycle, relating this auxin accumulation to new lateral roots development zones. In the same way, our results showed that the increased *pDR5::GFP* expression on the elongation and maturation zones of *A. thaliana* after azelaic acid treatment was related to auxin accumulation, favouring the new lateral root formation and consequently reducing auxin levels in the root tip. This hypothesis was further supported by our GC-MS analysis. The same occurred with the steroid saponin protodioscin, where auxin accumulation in the root pericycle (validated by auxin quantification) was related to lateral root initiation processes in the elongation zone (Santos Wagner et al., 2021). Similar results were reported by Bruno et al. (2021) after coumarin treatment, suggesting that coumarin probably promotes auxin accumulation, stimulating, as a stress response, enzymes involved in auxin catabolism.

In addition, AZA induced alterations in RAM organisation. The RAM size and width (also the number of cells that formed the proximal meristem) were reduced compared to the control, while the length of the cells was increased by the treatment (protodermis, precortex and proendodermis). Similar alterations were already observed in plants treated with other natural compounds, such as farnesene, coumarin or phroletin, suggesting the shortening of the meristematic zone and advancement of transition and differentiation zones (Araniti et al., 2017; Bruno et al., 2021; Smailagić et al., 2022). Furthermore, columella dimensions in AZA-treated roots (width, length and area) were lower than those of untreated roots. It is known that auxin plays an important role in the regulation of RAM architecture, and changes in auxin distribution or auxin levels can affect the root's size, shape and patterning (Gallavotti, 2013). Thus, AZA-induced changes in polar auxin transport, auxin biosynthesis or auxin signalling could lead to those alterations in the RAM structure, affecting the correct root development.

All the effects observed after AZA treatment, such as changes in the normal gravitropic response, disruptions in root architecture, abnormal elongation patterns, alterations in lateral root formation or changes in the auxin transport within the root (PIN proteins) could be related to alterations in the TIR1 complex (Arase et al., 2012). TIR1 (Transport Inhibitor Response 1) is an F-box protein that forms part of the SCF ubiquitin E3 ligase complex. Upon binding auxin, it interacts with specific transcriptional repressors (the Aux/IAA proteins) for ubiquitination by the SCF complex (Gomes and Scortecci, 2021). This process leads to the degradation of these repressors by the proteasome, activating the expression of specific auxin-responsive genes and disrupting normal growth and development (Leyser, 2018). Many auxinic herbicides, such as IAA (Indole-3-acetic acid), 1-NAA (1-Naphthaleneacetic acid), and 2,

4-D (2,4-Dichlorophenoxyacetic acid) have shown high binding affinity with the TIR1 complex (Christoffoleti et al., 2015). Similarly, the natural coumarin scopoletin has been suggested as a natural auxin herbicide that fits with the binding site of TIR1 (Transport Inhibitor Response 1) in *Arabidopsis* roots due to its structural similarities with the synthetic IAA analogue 2,4-D (Graña et al., 2017).

Molecular docking studies demonstrated that AZA binds with high affinity to TIR1 in the auxin binding pocket and competes for the binding site. Our results are in agreement with those described by Uzunova et al. (2016), who reported that in the binding of the hormone IAA to its receptor TIR1, interactions occurring along the depth of the auxin pocket are determinant for its stability. The authors highlight the role of residue Ser438, which, in the case of the AZA molecular docking, helped to strengthen the receptor binding through hydrogen bonds of carboxylate groups. They reported that Ser438 is physically located at the bottom of the pocket, which they consider to be responsible for the correct orientation of IAA.

Similarly, several residues identified in the computational simulation of AZA are identical to those highlighted in previous studies. For example, Ortiz-Castro et al. (2011) reported the auxinic activity of cyclodipeptides, highlighting the Arg489 residue in the TIR1 binding pocket. Recently, Yin et al. (2022) predicted by molecular docking analysis that residues of His78, Phe82, Leu378 and Ser438, among others, modulated *Arabidopsis thaliana* root system architecture by promoting interactions between TIR1 and IAA7/17 proteins.

Therefore, molecular docking simulations carried out in this study suggest that azelaic acid has an affinity for the auxin pocket of the TIR1 protein. The most important residues of the auxinic pocket could establish hydrogen bonds with AZA, and the flexible alkyl chain favoured hydrophobic interactions that stabilized the ligand-protein complex. Thus, if azelaic acid is acting as an auxinic herbicide, its binding with TIR1 could interfere with the normal functioning of the TIR1/AFB complex, disrupting the ubiquitin E3 ligase complex and leading to the downstream alterations on auxin signaling and gene expression that have been observed after AZA treatment (disruptions in root architecture, root elongation, auxin polar transport, gravitropic responses and/or lateral root formation). The presence of AZA, behaving as an auxinic compound, in the root meristem could be perceived by the plant as an excess of 'auxin', stopping the polar transport of auxin and accumulating this hormone in the upper parts of the root.

Wan et al. (2018) demonstrated that auxin accumulation in elongation and maturation zones is related to the inhibition of primary root elongation, as auxin reduces the expression of PINs transport proteins on the root apex, altering the correct polar auxin distribution. After 7 days of treatment, confocal microscopy images revealed that azelaic acid-treated roots experienced a generalized fall in the GFP fluorescence signal of PIN1, PIN2, PIN3, PIN4 and PIN7, accompanied by changes in the distribution of PIN2 and PIN4. Blilou et al. (2005) reported that losses in PIN1, PIN3 and PIN7 protein expression were related to reductions in primary root growth. Moreover, function losses of PIN2, responsible for the basipetal transport of auxin that is accumulated in the root apex, have been reported to cause auxin accumulation in the root tip (Zhang et al., 2019). As well treatment with the natural compound norharmane also showed alterations in *A. thaliana* seedlings since it inhibited the auxin polar transport of PIN2, PIN3 and PIN7 proteins by accumulating auxin in upper root areas without reaching the root cap and causing a significant increase of secondary and AR, as well as phytotoxic effects and a decrease in the growth of *A. thaliana* seedlings (López-González et al., 2020). In addition, the molecule farnesene strongly affected the auxin polar transport by reducing or inhibiting PIN proteins expression in root apical meristem (Araniti et al., 2017). In our work, azelaic acid also caused a reduction in both PIN2 expression and auxin signal in the root apex. This could be related to the fact that the expression of PIN1, PIN3, PIN4 and PIN7 efflux proteins, which are responsible for acropetal transport of auxin through the stele to the root apex, were also found to be reduced by azelaic acid, supporting the idea that AZA treatment could alter acropetal polar auxin transport from elongation zone to root tip, reducing auxin accumulation in root apex and causing inhibition of primary root elongation. Therefore, azelaic acid could alter the auxin distribution by reducing the auxin polar transport through PIN proteins.

5. Conclusion

In conclusion, this study has revealed azelaic acid's phytotoxic potential and its multifaceted effects on *Arabidopsis thaliana* root development. We have gained valuable insights into its mechanisms by analysing root morphology, anatomy, auxin dynamics, gravitropic response and molecular docking. Azelaic acid inhibits primary root growth while stimulating lateral and adventitious root formation, impacting the root apical meristem by reducing cell number, length, and width. It modulates auxin-related processes since computational simulations demonstrated that AZA has a high affinity for the auxin receptor TIR1, competing with the auxin binding site. AZA binding with TIR1 could interfere with the normal functioning of the TIR1/AFB complex, disrupting the ubiquitin E3 ligase complex, behaving as an auxinic herbicide and leading to increased auxin levels in the root, reduced transport to the meristematic zone, and accumulation in the elongation and maturation zones, aligning with observed morphological changes. This study underscores azelaic acid's phytotoxic action via auxin regulation, enriching our understanding of plant physiology and offering eco-friendly alternatives to synthetic herbicides, with the potential for targeted root growth manipulation in sustainable agriculture and plant management.

Funding

These results are part of the I+D+i project RT12018-094716-B-100 funded by MCIN/AEI/10.13039/501100011033, and part of the European EU-Horizon project "AGROSUS: AGROecological strategies for SUStainable weed management in key European crops" under grant agreement number 101084084. S.A-R was supported by a predoctoral fellowship of the Galician Government (ED481A-2021/328).

CRediT authorship contribution statement

Sara Álvarez-Rodríguez: Data curation, Formal analysis, Investigation, Writing – original draft, Writing – review & editing. **Fabrizio Araniti:** Conceptualization, Funding acquisition, Writing – original draft, Writing – review & editing. **Marta Teijeira:** Data curation, Formal analysis, Writing – original draft. **Manuel J. Reigosa:** Conceptualization, Funding acquisition. **Adela M. Sánchez-Moreiras:** Conceptualization, Funding acquisition, Writing – original draft, Writing – review & editing.

Declaration of competing interest

The authors declare that they have no known competing financial interests or personal relationships that could have appeared to influence the work reported in this paper.

Data availability

Data will be made available on request.

Acknowledgements

The authors would like to thank Catalina Sueiro and Inés Pazos from the Scientific and Technological Research Support Center (CACTI) of the Universidade de Vigo for their assistance in electron and confocal microscopy services. In addition, special thanks also to Dr. Jiří Friml from Institute of Science and Technology (IST), Austria, that gently provided

the *pPIN7::PIN7-GFP* transgenic line used in the experiments.

References

Abagyan, R., Totrov, M., 1994. Biased probability Monte Carlo conformational searches and electrostatic calculations for peptides and proteins. J. Mol. Biol. 235 (3), 983–1002.

Abas, L., Kolb, M., Stadlmann, J., Janacek, D.P., Lukic, K., Schwechheimer, C., Sazanov, L.A., Mach, L., Friml, J., Hammes, U.Z., 2021. Naphthylphthalamic acid associates with and inhibits PIN auxin transporters. Proc. Natl. Acad. Sci. 118 (1), e2020857118.

Alarcón, M.V., Salguero, J., Lloret, P.G., 2019. Auxin modulated initiation of lateral roots is linked to pericycle cell length in maize. Front. Plant Sci. 10, 11.

Álvarez-Rodríguez, S., López-González, D., Reigosa, M.J., Araniti, F., Sánchez-Moreiras, A.M., 2022. Ultrastructural and hormonal changes related to harmaline-induced treatment in *Arabidopsis thaliana* (L.) Heynh. root meristem. Plant Physiol. Biochem. 179, 78–89.

Andriana, Y., Xuan, T.D., Quan, N.V., Quy, T.N., 2018. Allelopathic potential of *Tridax procumbens* L. on radish and identification of allelochemicals. Allelopathy J. 43, 223–238.

Araniti, F., Bruno, L., Sunseri, F., Pacenza, M., Forgione, I., Bitonti, M.B., Abenavoli, M. R., 2017. The allelochemical farnesene affects *Arabidopsis thaliana* root meristem altering auxin distribution. Plant Physiol. Biochem. 121, 14–20.

Araniti, F., Talarico, E., Madeo, M.L., Greco, E., Minervino, M., Álvarez-Rodríguez, S., Muto, A., Ferrari, M., Chiappetta, A., Bruno, L., 2023. Short-term exposition to acute Cadmium toxicity induces the loss of root gravitropic stimuli perception through PIN2-mediated auxin redistribution in *Arabidopsis thaliana* (L.) Heynh. Plant Sci. 111726.

Arase, F., Nishitani, H., Egusa, M., Nishimoto, N., Sakurai, S., Sakamoto, N., Kaminaka, H., 2012. IAA8 involved in lateral root formation interacts with the TIR1 auxin receptor and ARF transcription factors in *Arabidopsis*. PLoS One 7 (8), e43414.

Balzan, S., Johal, G.S., Carraro, N., 2014. The role of auxin transporters in monocots development. Front. Plant Sci. 5, 393.

Blilou, I., Xu, J., Wildwater, M., Willemsen, V., Paponov, I., Friml, J., Heidstra, R., Aida, M., Palme, K., Scheres, B., 2005. The PIN auxin efflux facilitator network controls growth and patterning in *Arabidopsis* roots. Nature 433 (7021), 39–44.

Boerjan, W., Cervera, M.T., Delarue, M., Beeckman, T., Dewitte, W., Bellini, C., Caboche, M., Onckelen, H.V., Montagu, M.V., Inze, D., 1995. Superroot, a Recessive mutation in *Arabidopsis*, confers auxin overproduction. Plant Cell Online 7 (9), 1405–1419.

Brenna, E., Colombo, D., Di Lecce, G., Gatti, F.G., Ghezzi, M.C., Tentori, F., Tessaro, D., Viola, M., 2020. Conversion of oleic acid into azelaic and pelargonic acid by a chemo-enzymatic route. Molecules 25 (8), 1882.

Bruno, L., Talarico, E., Cabeiras-Freijanes, L., Madeo, M.L., Muto, A., Minervino, M., Lucini, L., Miras-Moreno, B., Sofo, A., Araniti, F., 2021. Coumarin interferes with polar auxin transport altering microtubule cortical array organization in *Arabidopsis thaliana* (L.) Heynh. root apical meristem. Int. J. Mol. Sci. 22 (14), 7305.

Cecchini, N.M., Roychoudhry, S., Speed, D.J., Steffes, K., Tambe, A., Zodrow, K., Konstantinoff, K., Jung, H.W., Engle, N.L., Tschaplinski, T.J., Greenberg, J.T., 2019. Underground azelaic acid–conferred resistance to *Pseudomonas syringae* in *Arabidopsis*. Mol. Plant Microbe Interact. 32 (1), 86–94.

Christoffoleti, P.J., Figueiredo, M.R.A.D., Peres, L.E.P., Nissen, S., Gaines, T., 2015. Auxinic herbicides, mechanisms of action, and weed resistance: a look into recent plant science advances. Sci. Agric. 72, 356–362.

De Rybel, B., Audenaert, D., Xuan, W., Overvoorde, P., Strader, L.C., Kepinski, S., Hoye, R., Brisbois, R., Parizot, B., Vanneste, S., Liu, X., Gilday, A., Graham, I.A., Nguyen, L., Jansen, L., Njo, M.F., Inzé, D., Bartel, B., Beeckman, T., 2012. A role for the root cap in root branching revealed by the non-auxin probe naxillin. Nature Chem. Biol. 8 (9), 798–805.

Delarue, M., Prinsen, E., Onckelen, H.V., Caboche, M., Bellini, C., 1998. *Sur2* mutations of *Arabidopsis thaliana* define a new locus involved in the control of auxin homeostasis. Plant J. 14 (5), 603–611.

Díaz-Tielas, C., Graña, E., Sotelo, T., Reigosa, M.J., Sánchez-Moreiras, A.M., 2012. The natural compound trans-chalcone induces programmed cell death in *Arabidopsis thaliana* roots. Plant Cell Environ. 35 (8), 1500–1517.

Gallavotti, A., 2013. The role of auxin in shaping shoot architecture. J. Experim. Bot. 64 (9), 2593–2608.

Gomes, G.L.B., Scortecci, K.C., 2021. Auxin and its role in plant development: structure, signalling, regulation and response mechanisms. Plant Biol 23 (6), 894–904.

Gonin, M., Bergougnoux, V., Nguyen, T.D., Gantet, P., Champion, A., 2019. What makes adventitious roots? Plants 8 (7), 240.

Graña, E., Costas-Gil, A., Longueira, S., Celeiro, M., Teijeira, M., Reigosa, M.J., Sánchez-Moreiras, A.M., 2017. Auxin-like effects of the natural coumarin scopoletin on *Arabidopsis* cell structure and morphology. J. Plant Physiol. 218, 45–55.

Graña, E., Sotelo, T., Díaz-Tielas, C., Araniti, F., Krasuska, U., Bogatek, R., Reigosa, M.J., Sánchez-Moreiras, A.M., 2013. Citral induces auxin and ethylene-mediated malformations and arrests cell division in *Arabidopsis thaliana* roots. J. Chem. Ecol. 39, 271–282.

Grossmann, K., Tresch, S., Plath, P., 2001. Triaziflam and diaminotriazine derivatives affect enantioselectively multiple herbicide target sites. Z. Naturforsch. C 56 (7–8), 559–569.

Huang, A., Wang, Y., Liu, Y., Wang, G., She, X., 2020. Reactive oxygen species regulate auxin levels to mediate adventitious root induction in *Arabidopsis* hypocotyl cuttings. J. Integr. Plant Biol. 62 (7), 912–926.

Jung, H.W., Tschaplinski, T.J., Wang, L., Glazebrook, J., Greenberg, J.T., 2009. Priming in systemic plant immunity. Science 324 (5923), 89–91.

Landi, M., Misra, B.B., Muto, A., Bruno, L., Araniti, F., 2020. Phytotoxicity, morphological, and metabolic effects of the sesquiterpenoid nerolidol on *Arabidopsis thaliana* seedling roots. Plants 9 (10), 1347.

Leyser, O., 2018. Auxin signaling. Plant Physiol 176 (1), 465–479.

López-González, D., Costas-Gil, A., Reigosa, M.J., Araniti, F., Sánchez-Moreiras, A.M., 2020. A natural indole alkaloid, norharmane, affects PIN expression patterns and compromises root growth in *Arabidopsis thaliana*. Plant Physiol. Biochem. 151, 378–390.

Ma, Y., Chun, J., Wang, S., Chen, F., 2011. Allelopathic potential of *Jatropha curcas*. Afr. J. Biotechnol. 10 (56), 11932–11942.

Oono, Y., Ooura, C., Rahman, A., Aspuria, E.T., Hayashi, K.I., Tanaka, A., Uchimiya, H., 2003. *p*-Chlorophenoxyisobutyric acid impairs auxin response in *Arabidopsis* root. Plant Physiol. 133(3), 1135-1147.

Ortiz-Castro, R., Díaz-Pérez, C., Martínez-Trujillo, M., del Río, R.E., Campos-García, J., López-Bucio, J., 2011. Transkingdom signaling based on bacterial cyclodipeptides with auxin activity in plants. Proc. Natl. Acad. Sci. 108 (17), 7253–7258.

Prusinska, J., Uzunova, V., Schmitzer, P., Weimer, M., Bell, J., Napier, R.M., 2023. The differential binding and biological efficacy of auxin herbicides. Pest Manag. Sci. 79 (4), 1305–1315.

Qu, R.Y., He, B., Yang, J.F., Lin, H.Y., Yang, W.C., Wu, Q.Y., Li, Q.X., Yang, G.F., 2021. Where are the new herbicides? Pest Manag. Sci. 77 (6), 2620–2625.

Rashotte, A.M., Brady, S.R., Reed, R.C., Ante, S.J., Muday, G.K., 2000. Basipetal auxin transport is required for gravitropism in roots of *Arabidopsis*. Plant Physiol 122 (2), 481–490.

Rawlinson, C., Kamphuis, L.G., Gummer, J.P., Singh, K.B., Trengove, R.D., 2015. A rapid method for profiling of volatile and semi-volatile phytohormones using methyl chloroformate derivatisation and GC–MS. Metabolomics 11, 1922–1933.

Sánchez-Moreiras, A.M., Pacenza, M., Araniti, F., Bruno, L., 2018. Confocal and transmission electron microscopy for plant studies. In: Sánchez-Moreiras, A.M., Reigosa, M.J. (Eds.), Advances in Plant Ecophysiology Techniques. Springer, pp. 253–271.

Santos Wagner, A.L., Araniti, F., Bruno, L., Ishii-Iwamoto, E.L., Abenavoli, M.R., 2021. The steroid saponin protodioscin modulates *Arabidopsis thaliana* root morphology altering auxin homeostasis, transport and distribution. Plants 10 (8), 1600.

Schulz, B., Segobye, K., 2016. 2, 4-D transport and herbicide resistance in weeds. J. Exp. Bot. 67 (11), 3177–3179.

Sharma, N., Tiwari, N., Vyas, M., Khurana, N., Muthuraman, A., Utreja, P., 2020. Pharmacological activities of azelaic acid: a recent update. Plant Arch 20, 3048–3052.

Searle, T., Ali, F.R., Al-Niaimi, F., 2022. The versatility of azelaic acid in dermatology. J. Dermatol. Treat. 33 (2), 722–732.

Smailagić, D., Banjac, N., Ninković, S., Savić, J., Ćosić, T., Pěnčík, A., Ćalić, D., Bogdanović, M., Trajković, M., Stanišić, M., 2022. New Insights into the activity of apple dihydrochalcone phloretin: disturbance of auxin homeostasis as physiological basis of phloretin phytotoxic action. Front. Plant Sci. 13.

Song, Y., 2014. Insight into the mode of action of 2, 4-dichlorophenoxyacetic acid (2, 4-D) as an herbicide. J. Int. Plant Biol. 56 (2), 106–113.

Truernit, E., Bauby, H., Dubreucq, B., Grandjean, O., Runions, J., Barthélémy, J., Palauqui, J.C., 2008. High-resolution whole-mount imaging of three-dimensional tissue organization and gene expression enables the study of phloem development and structure in *Arabidopsis*. Plant Cell 20 (6), 1494–1503.

Uzunova, V.V., Quareshy, M., Del Genio, C.I., Napier, R.M., 2016. Tomographic docking suggests the mechanism of auxin receptor TIR1 selectivity. Open Biol. 6 (10), 160139.

Wan, J., Zhang, P., Sun, L., Li, S., Wang, R., Zhou, H., Wang, W., Xu, J., 2018. Involvement of reactive oxygen species and auxin in serotonin-induced inhibition of primary root elongation. J. Plant Physiol. 229, 89–99.

Yin, L., Chen, X., Chen, Q., Wei, D., Hu, X.Y., Jia, A.Q., 2022. Diketopiperazine modulates *Arabidopsis thaliana* Root System Architecture by promoting interactions of auxin receptor TIR1 and IAA7/17 proteins. Plant Cell Physiol. 63 (1), 57–69.

Zhang, Y., He, P., Ma, X., Yang, Z., Pang, C., Yu, J., Wang, G., Friml, J., Xiao, G., 2019. Auxin-mediated statolith production for root gravitropism. New Phytol. 224 (2), 761–774.

Zhou, L., Hou, H., Yang, T., Lian, Y., Sun, Y., Bian, Z., Wang, C., 2018. Exogenous hydrogen peroxide inhibits primary root gravitropism by regulating auxin distribution during *Arabidopsis* seed germination. Plant Physiol. Biochem. 128, 126–133.